European Journal of Medicinal Chemistry 199 (2020) 112388

Contents lists available at ScienceDirect

European Journal of Medicinal Chemistry

journal homepage: http://www.elsevier.com/locate/ejmech

Research paper

Discovery of new thieno[3,2-*d*]pyrimidine derivatives targeting EGFR$^{L858R/T790M}$ NSCLCs by the conformation constrained strategy

Yang Chen [a, 1], Linlin Yang [b, 1], Hui Qiao [a], Zhongyu Cheng [a], Jiahao Xie [a], Wenjuan Zhou [a], Xin Huang [a], Yaoxuan Jiang [a], Bin Yu [a, **], Wen Zhao [a, *]

[a] State Key Laboratory of Esophageal Cancer Prevention and Treatment, Key Laboratory of Advanced Pharmaceutical Technology, Ministry of Education of China, School of Pharmaceutical Sciences, Zhengzhou University, Zhengzhou, Henan, 450001, PR China
[b] Department of Pharmacology, School of Basic Medical Sciences, Zhengzhou University, Zhengzhou, 450001, PR China

ARTICLE INFO

Article history:
Received 18 December 2019
Received in revised form
23 April 2020
Accepted 23 April 2020
Available online 4 May 2020

Keywords:
Thieno[3,2-*d*]pyrimidine
Quinolin-2(1*H*)-Ones
EGFR inhibitors
Lung cancer

abstract

Studies on the third-generation of epidermal growth factor receptor tyrosine kinase inhibitors (EGFR-TKIs) targeting EGFR$^{L858R/T790M}$ mutant remain hotspots, specifically for non-small cell lung cancer (NSCLC). In the current study, a new series of EGFR-TKIs with thieno[3,2-*d*]pyrimidine derivatives(**6a-6r)** bearing quinolin-2(1*H*)-ones were designed and synthesized, through conformational constrained strategy from the third generation of EGFR-TKI olmutinib. *In vitro* structure-activity relationship (SAR) studies indicated that compounds **6a**, **6l**, **6m**, **6n** and **6o** exhibited good selective inhibition to EGFR$^{L858R/T790M}$ ($IC_{50} \leq 250$ nM) over wild type EGFR ($IC_{50} > 10000$ nM). The observed selectivity of compounds **6l** and **6o** was also proved by the computational molecular docking and the cellular thermal shift assay. These compounds had good growth inhibitory effect on the four tested cancer cell lines. Specifically, **6o** could significantly inhibit the colony formation, wound healing and the expression of p-EGFR and its downstream p-ERK in EGFR$^{L858R/T790M}$ H1975 lung cancer cells. Our findings suggest that the thieno[3,2-d]pyrimidine compounds, especially **6l** and **6o**, can selectively target the mutant EGFR$^{L858R/T790M}$ in vitro and at cellular level and may serve as the lead compounds for generating new series of the third-generation EGFR-TKIs.

1. Introduction

Non-small-cell lung cancer (NSCLC) accounts for approximately 80% of lung cancer screening (LCs), which is an extremely serious threat to human health, with the highest mortality rates among cancers all over the world [1–3]. EGFR overexpression and associated mutations (L858R mutation and exon-19 deletion) are closely linked to NSCLC's tumorigenesis. Targeted inhibition of EGFR and its mutants is one of the promising strategies for the treatment of NSCLCs [4]. The first-line targeted drugs for NSCLC clinical therapy include the first-generation of gefitinib [5], erlotinib [6] and the second-generation afatinib [7], both of which target EGFR^{del19} and EGFR^{L858R} mutations and have achieved significant clinical response rate in NSCLC patients [8]. However, about 60% patients occurred EGFR^{T790M} resistance mutation during 9–14 months treatment of first-generation [9,10]. These EGFR tyrosine-kinase inhibitors (EGFR-TKIs) can also bring severe adverse events (such as rash, paronychia, fissuring, desquamation and pruritus) in patients, due to the activity against wild-type EGFR, which is widely distributed on mammalian epithelial cells, fibroblasts, glial cells, keratinocytes and plays a physiological role in skin and gastrointestinal tissues [11–14]. Therefore, the third-generation of EGFR inhibitors have been developed (Fig. 1), including: osimertinib (AZD9291) [15], olmutinib, PF06747775, avitinib, nazartinib, AZ5104, WZ4002 and others [16], not only with good inhibition targeting EGFR^{T790M} mutation, but also with good selectivity over EGFR^{WT} [16,17]. However, the commercially available third-generation of EGFR inhibitors have been proved to exhibit some side effects in the clinical setting, including severe skin ulceration and rash [18–20]. Development of new third-generation EGFR

* Corresponding author. School of Pharmaceutical Sciences Zhengzhou University Zhengzhou, Henan, 450001, PR China.
** Corresponding author. School of Pharmaceutical Sciences Zhengzhou University Zhengzhou, Henan, 450001, PR China.
E-mail addresses: yubin@zzu.edu.cn (B. Yu), zhaowen100@139.com, zhaowen@zzu.edu.cn (W. Zhao).
[1] These authors contribute equally to this work.

https://doi.org/10.1016/j.ejmech.2020.112388
0223-5234/

inhibitors with high selectivity and low toxicity is still highly needed [21]. Fourth-generation EGFR inhibitors have been designed and synthesized, including EAI-045 [22,23]. The fourth generation of EGFR inhibitors, also known as allosteric inhibitors, mainly changes the conformation of EGFR by binding to EGFR, making it unable to bind to ATP, and eventually loses its catalytic effect. The fourth-generation EGFR inhibitor overcomes the EGFR C797S resistance mutation of the third-generation inhibitor. However, there are few studies on fourth-generation EGFR inhibitors and there are no effective fourth-generation EGFR inhibitors in clinical studies. Development of new third- and fourth-generation EGFR inhibitors with high selectivity and low toxicity is still highly needed [21]. Therefore, we herein report the discovery of potent and selective thieno[3,2-*d*]pyrimidine derivatives from the third-generation EGFR inhibitor olmutinib based on the conformational constrained strategy (Fig. 2). Interestingly, we found that some of these compounds exhibited EGFR inhibition and cytotoxic effects against several human cancer cell lines. Particularly, compound **6o** exhibited potent and selective inhibition for lung adenocarcinoma cell H1975 lines bearing $EGFR^{L858R/T790M}$ mutation. Our related work have obtained the invention patent certificate [24].

2. Results and discussion

2.1. Chemistry

The synthetic route of compounds **6a-r** is shown in Scheme 1. 3-methoxyaniline (**1**) reacted with cinnamoyl chloride (**2**) in the presence of K_2CO_3 in a mixed solution of acetone and water at 0 °C to form compound **3**. With the $AlCl_3$ suspended in chlorobenzene, compound **3** was converted to 7-hydroxyquinolin-2(1*H*)-one (**4**). Treatment of 7-hydroxyquinolin-2(1*H*)-one with 2,4-dichlorothieno[3,2-*d*]pyrimidine in the presence of K_2CO_3 in acetonitrile gave compound **5**, which was then subjected to the Pd-catalyzed coupling reactions, forming the desired compounds **6a-r**.

2.2. Kinase inhibition of $EGFR^{L858R/T790M}$ and $EGFR^{WT}$

The kinase inhibition of these compounds against $EGFR^{L858R/T790M}$ and $EGFR^{WT}$ were evaluated, using olmutinib, AZD9291 and afatinib as positive controls (**Table 1**). Some of the compounds inhibited $EGFR^{L858R/T790M}$ potently with the IC_{50} values ranging from 110 to 330 nM, while the corresponding IC_{50} values for $EGFR^{WT}$ were >10 μM. Of these compounds, **6l** displayed the best potency on $EGFR^{L858R/T790M}$ with an IC_{50} value of 110 nM. However, replacement of the phenyl ring with the pyridine ring led to decrease of the activity (**6a** *vs*. **6p**). Compounds **6l** and **6o** inhibited $EGFR^{WT}$ with the IC_{50} values of 12.43 and 13.97 μM, respectively, indicating their higher selectivity to $EGFR^{L858R/T790M}$ (selectivity indexes were 113 and 61, respectively) (Fig. 3A, B, C and D) than that in olmutinib (selectivity index 46) (Fig. 3E and F).

We also found that compared to **6a**, compounds **6b**, **6e** and **6i** bearing the morpholine group showed decreased inhibitory activity against $EGFR^{L858R/T790M}$. *N*-Methyl and *N*-ethyl piperazine substituted compounds **6c** and **6d** were completely inactive against $EGFR^{L858R/T790M}$, suggesting the importance of the phenyl ring for the activity. As shown in Table 1, compounds **6f**, **6g**, **6j-o** showed comparable inhibitory activity with **6a**. Compound 6p inhibited $EGFR^{L858R/T790M}$ with an inhibitory rate of 32% at 1.0 μM. Additionally, removal of the hydrophilic group (e.g. piperazine, etc.) caused significant loss of the activity. Compounds **6q** and **6r** inhibited $EGFR^{L858R/T790M}$ with the inhibitory rates of 8% and 22%, respectively at 1.0 μM, significantly lower than that of **6a**, unveiling the importance of the hydrophilic group for the activity. For wild type EGFR, all of these compounds exhibited weak activity with IC_{50} more than 10 μM (Table 1)

2.3. Molecular docking

Molecular docking studies for compounds **6l** and **6o** were then performed to reveal the structural basis for the selectivity. The crystal structures of 4-(4-{[2-{[(3S)-1-acetylpyrrolidin-3-yl]amino}-9-(propan-2-yl)-9*H*-purin-6-yl]amino}phenyl)-1-methylpiperazin-1-ium (a reversible $EGFR^{L858R/T790M}$ inhibitor) in a complex with $EGFR^{L858R/T790M}$ mutant (PDB ID: 5UGA) and $EGFR^{WT}$ (PDB ID: 5UGB) [25] were chosen as the docking receptors, considering the structural similarity of this inhibitor with our compounds **6l** and **6o**.

In $EGFR^{WT}$, **6l** and **6o** adopted an "U-shaped" conformation like olmutinib (Fig. 4A and C, Fig. 5A). Compared with the Michael acceptor in olmutinib, both **6l** and **6o** had quinolinone groups, which could also covalently bind to C797 and made hydrophobic interactions with L844. Similar to olmutinib, the thieno[2,3-*d*]pyrimidine core of **6l** and **6o** was pointed to the inner pocket, forming hydrophobic interactions with L718, A743 and V726, and the amino pyrimidine group formed two hydrogen bonds with the main-chain

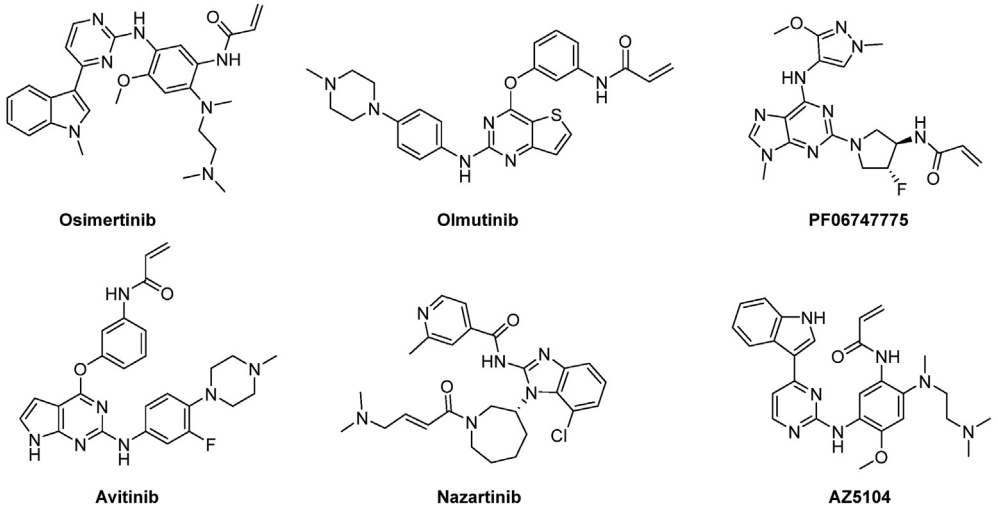

Fig. 1. Representative third-generation EGFR-TKIs.

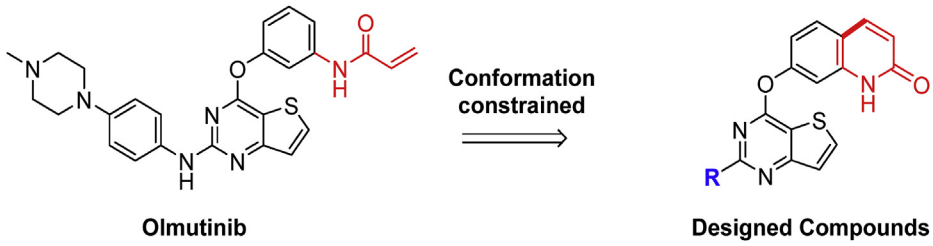

Fig. 2. Discovery of thieno[3,2-*d*]pyrimidine derivatives as new EGFR$^{L858R/T790M}$ inhibitors from olmutinib based on the conformational constrained strategy.

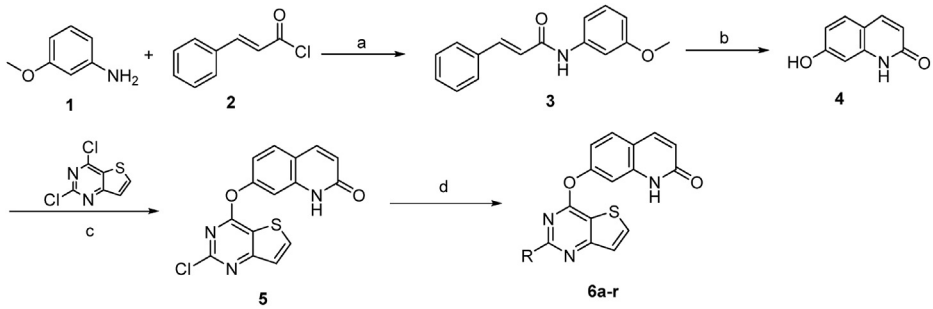

Scheme 1. Synthesis of thieno[3,2-*d*]pyrimidine derivatives. Reagents and conditions: (a) K_2CO_3, acetone, H_2O, 0 °C, 30 min; (b) $AlCl_3$, chlorobenzene, reflux, 120 °C, 3–5 h; (c) K_2CO_3, MeCN, H_2O, 60 °C, 2–5 h; (d) amines, Cs_2CO_3, dioxane, $Pd_2(dba)_3$, BINAP, reflux, 3–5 h.

atoms of M793 in the hinge region. The steric *para*-substituted aniline group extended in the inner pocket. Different from olmutinib, **6l** and **6o** made additional polar interactions with E804 or D800.

In EGFR$^{L858R/T790M}$, **6l** and **6o** maintained the same binding pose as in EGFR^{WT} (Fig. 4B and D). The bulky side chain of T790M mutation increased hydrophobic interactions with the thieno[2,3-*d*] pyrimidine scaffold. More than that, the conformation of the activation loop was significantly changed by the L858R mutation, allowing F856 to form hydrophobic interactions with the quinolinone group. As has been reported, the conformational changes of the activation loop affected the conformation of nearby αC-helix, making EGFR in an inactive state. These additional hydrophobic interactions improved the binding affinity of **6l** and **6o** to EGFR$^{L858R/T790M}$, contributing to their inhibitory selectivity of EGFR$^{L858R/T790M}$ over EGFR^{WT}. However, for olmutinib, due to the weak interactions between its steric *para*-substituted aniline group and the inner pocket, this group was directed to the outside of the pocket to form hydrophobic interactions with F856 in EGFR$^{L858R/T790M}$ (Fig. 5B). Though both M790 and F856 formed additional hydrophobic interactions with olmutinib in EGFR$^{L858R/T790M}$, olmutinib had less hydrogen bonds with M793 and R841 in this new binding mode, which might explain its worse selectivity to EGFR$^{L858R/T790M}$ than **6l** and **6o**.

Our docking studies showed that compounds **6l** and **6o** could form more polar interactions in the inner pocket than olmutinib, and made more hydrophobic interactions with both M790 and the conformationally changed activation loop caused by L858R, stabilizing the inactive conformation of EGFR. Consistent with our findings, previously reported X-ray co-crystal structures also revealed that L858R mutation could induce changes of activation loop, αC-helix and small molecule binding conformations [25–28]. Therefore, we speculate that structural changes of the steric *para*-substituted aniline group to form more polar or hydrophobic interactions with the inner pocket, and changes of the thieno[2,3-d] pyrimidine scaffold and quinolinone groups to increase hydrophobic interactions with M790 and the activation loop may be a feasible strategy to design selective small-molecule inhibitors targeting EGFR$^{L858R/T790M}$.

2.4. Cellular target engagement of compounds **6l** and **6o** with EGFR

To further determine whether **6o** and **6l** could bind to intracellular EGFR, the cellular thermal shift assay (CETSA) was performed in H1975 (expressing EGFR$^{L858R/T790M}$) and A549 (expressing EGFR^{WT}) cell lines (Fig. 6). The results showed that relative to the Dimethyl sulfoxide (DMSO) control, treatment with **6l** and **6o** resulted in significant increases in the protein signals with the enhanced temperature to 64 °C in H1975 cells (Fig. 6A), suggesting the thermal stability and the cellular target engagement of EGFR by these two compounds. However, in A549 cells, treatment with compounds **6l** and **6o** exhibited almost no signals in EGFRs (Fig. 6B). The data indicated that both compounds 6l and 6° had a good targeted binding effect on mutant EGFR protein at the cellular level.

2.5. Anti-proliferative activity

The cytotoxicity of the synthesized compounds were evaluated in four different cancer cell lines, including H1975 (EGFR$^{L858R/T790M}$), A549 (EGFR^{WT}), PC9 (EGFR^{del19}), and human normal liver cell line L02, using the MTT assay. The well-known anticancer drug gefitinib, erlotinib, and olmutinib were employed as the positive controls (Table 2).

Most of the tested compounds had moderate to good antiproliferative activity against the tested cancer cell lines. In contrast, these compounds showed relatively weak inhibition against normal human liver cell line L02, suggesting that these compounds have low toxicity in normal cells. The effects of compound **6o** on the cell viability of H1975 and A549 cells are shown in Fig. 7.

Table 1
Inhibitory activity of compounds **6a-r** against $EGFR^{L858R/T790M}$ and $EGFR^{W.T.}$.

Comp.	R	$EGFR^{L858R/T790M}$		$EGFR^{WT}$	Selectivity
		% inhibition at 1 μM	IC_{50} (μM)	IC_{50} (μM)	
6a	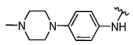	82	0.25 ± 0.04	>10	>40
6b	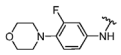	39	>1	>10	
6c		inactive	>1	ND[a]	
6d		inactive	>1	>10	
6e	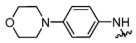	56	ND	>10	
6f	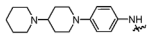	83	ND	>10	
6g	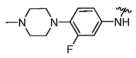	82	ND	>10	
6h	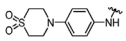	64	ND	>10	
6i	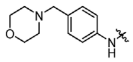	60	ND	>10	
6j	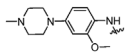	74	0.33 ± 0.01	>10	>30
6k	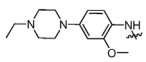	75	0.33 ± 0.01	>10	>30
6l	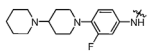	87	0.11 ± 0.01	12.43 ± 0.23	113
6m	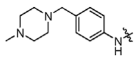	83	0.20 ± 0.01	>10	>50
6n	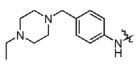	81	0.24 ± 0.03	>10	>42
6o	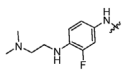	81	0.23 ± 0.03	13.97 ± 4.93	61
6p	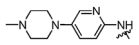	32	>1	>10	
6q	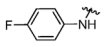	8	>1	>10	
6r	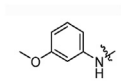	22	>1	>10	
Olmutinib			0.0009	0.039 ± 0.002	43
AZD9291			0.0006 ± 0.0002	ND	
Afatinib			ND	0.00024 ± 0.00005	

[a] ND means no determined.

2.6. Compound **6o** inhibited colony formation of H1975 and A549 cells

Because there are literatures showing that EGFR regulates the proliferation and invasion of tumor cells. Clonal formation experiment is an important technique for detecting cell proliferation and invasion, so we tested whether the compound 6° inhibits the ability of H1975 and A549 cells to form clones [29,30]. In view of the potency of **6o**, we then analyzed the effect of **6o** on the cell proliferation by colony formation assay (Fig. 8). Treatment with **6o** in H1975 cells significantly inhibited colony formation in a dose-dependent manner. In contrast, compound **6o** also inhibited colony formation of A549, albeit with less potency. The results demonstrated that **6o** was more sensitive to H1975 cells.

2.7. Compound **6o** inhibited the migration ability of H1975 cells more effectively

To study the effects of compound **6o** on tumor cell migration, wound Healing assays in H1975 and A549 cell lines were performed. In H1975 cells, the migration rate was decreased significantly with the increase of the concentration of **6o**. After 48 h administration at 5 μM, the migration rate was only about 0.03 (Fig. 9A and 9B). While in A549 cells, the migration rate was not

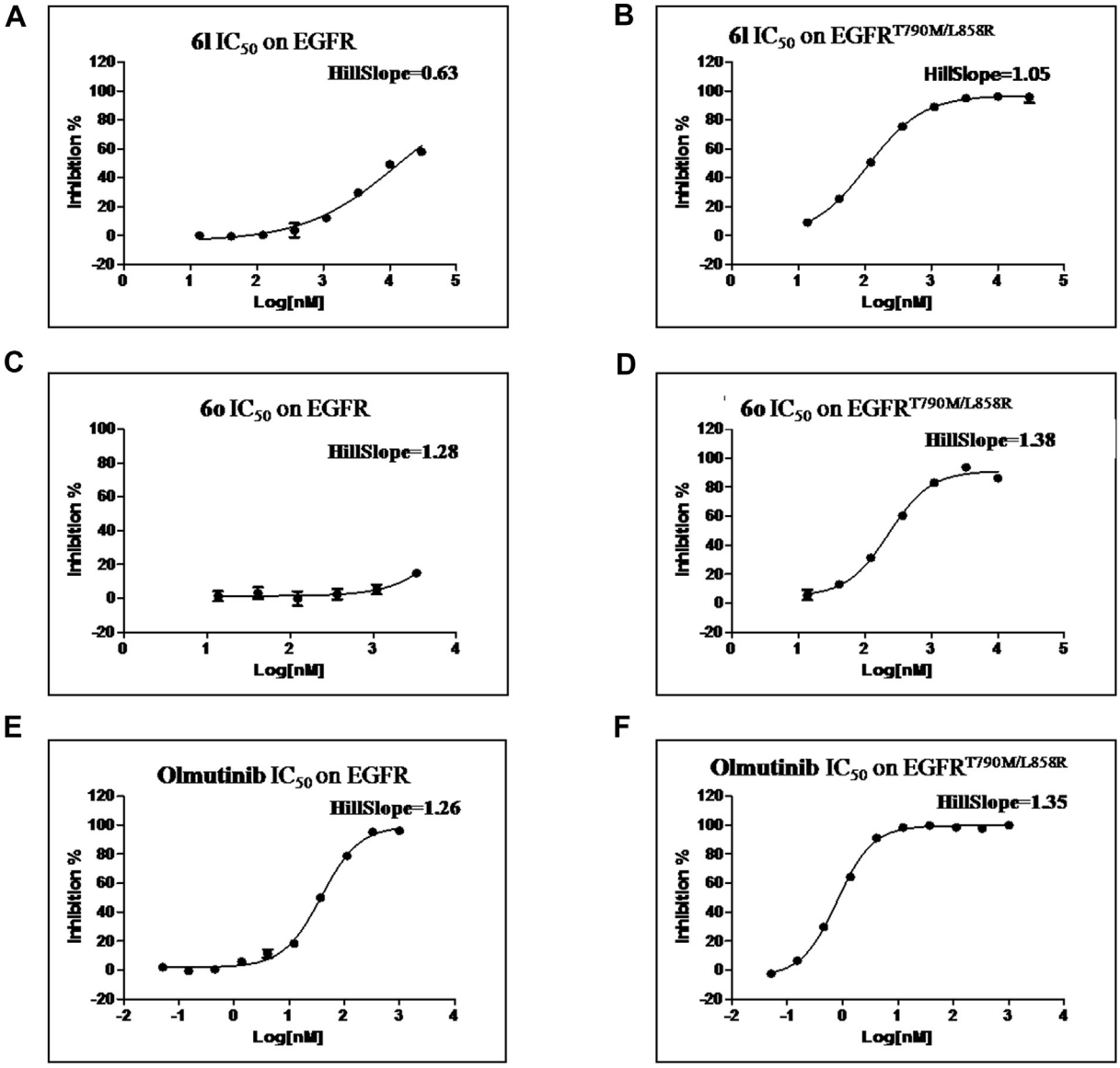

Fig. 3. Compound **6l, 6o** and Olmtinib combines with EGFR and inhibits EGFR activity. Compound **6l** (A and B)**, 6o** (C and D) and Olmtinib (E and F) were added into the screening systems and its inhibition rates (%) at different concentration were determined. Data are presented as means ± SD. Three individual experiments were performed for each group.

decreased obviously, and there was still 0.24 after 48 h administration of **6o** at 5 μM. The results indicated that **6o** was more effective for inhibiting the migration in H1975 cells.

*2.8. Compound **6o** blocked EGFR signaling pathways in H1975 cells*

Upon consideration of the inhibitory activities against $EGFR^{L858R/T790M}$, its downstream proteins and anti-proliferative effects by **6o** in H1975 cells, we detected the expression of key proteins in the EGFR signaling pathway. We found that after **6o** treatment, the p-EGFR and p-ERK expression levels were decreased about 34, 43, 89% and 5, 53, 66%, respectively, in a dose dependent manner (Fig. 10A, B and C). While in A549 cells, the expression of p-EGFR and p-ERK were not significant changed (Fig. 10D, E and F). These findings indicated that compound **6o** could more specifically target the mutant EGFR and its related downstream phosphorylated protein expression.

3. Conclusion

In the current study, 18 novel thieno[3,2-*d*]pyrimidine derivatives **6a-6r** bearing quinolin-2(1*H*)-ones were designed and synthesized from the third-generation EGFR inhibitor olmutinib. Among them, compounds **6l** and **6o** were more selective to $EGFR^{L858R/T790M}$ over wild type EGFR, not only proved by the in vitro assay and the cellular EGFR signaling evaluation, but also mimicked by the computer based molecular docking. Furthermore, compound **6o** could also significantly inhibit the colony formation, wound healing and the expression of p-EGFR and its downstream p-ERK in H1975 cells. These findings suggest that the thieno[3,2-d]

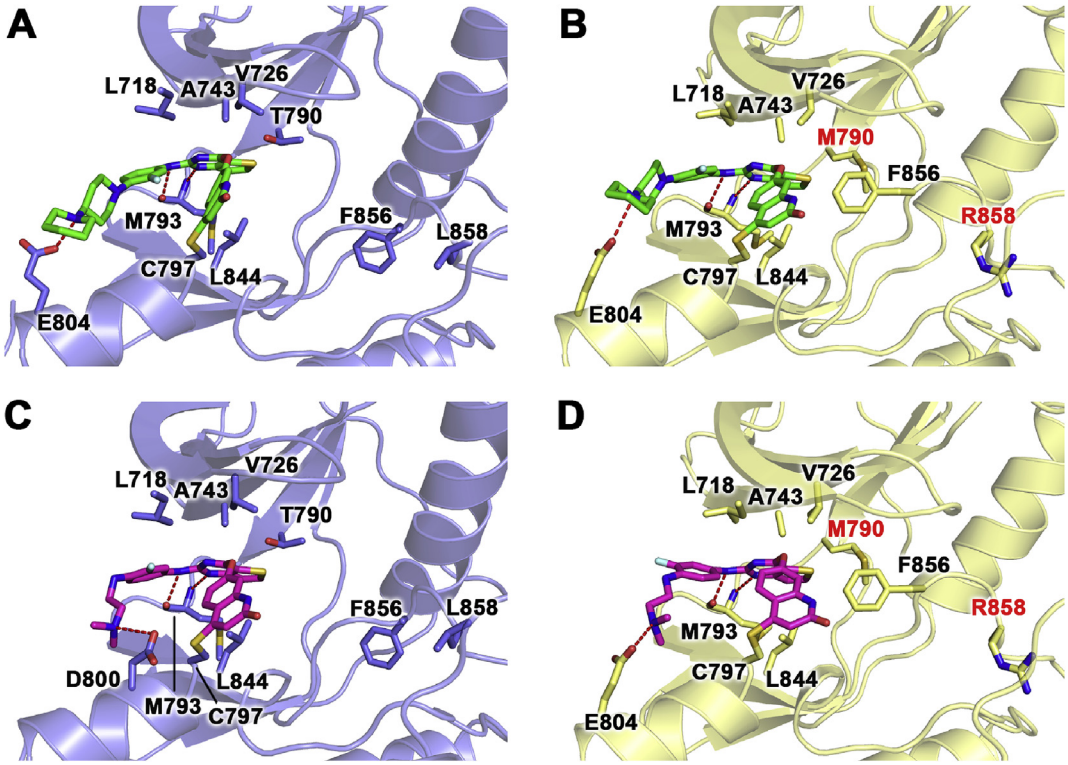

Fig. 4. Binding modes of compounds **6l** and **6o** in the wild-type (slate) and L858R/T790M mutant (yellow) EGFR kinases. Residues involved in interactions with **6l** (green, A and B) and **6o** (magenta, C and D) are depicted as sticks and labeled. For clarity, only side chains are shown and the two mutation sites T790M and L858R are labeled in red. Polar interactions are indicated with red dashed lines. (For interpretation of the references to colour in this figure legend, the reader is referred to the Web version of this article.)

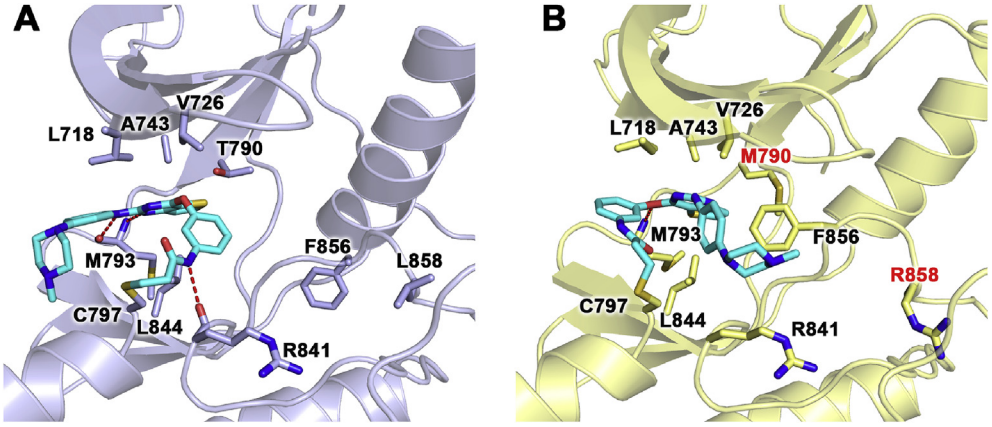

Fig. 5. Olmutinib (cyan) binding modes in the wild-type (slate) and L858R/T790M mutant (yellow) EGFR kinase. Residues involved in interactions with olmutinib are depicted as sticks and labeled. For clarity, only side chains are shown and the two mutation sites T790M and L858R are labeled in red. Polar interactions are indicated with red dashed lines. (For interpretation of the references to colour in this figure legend, the reader is referred to the Web version of this article.)

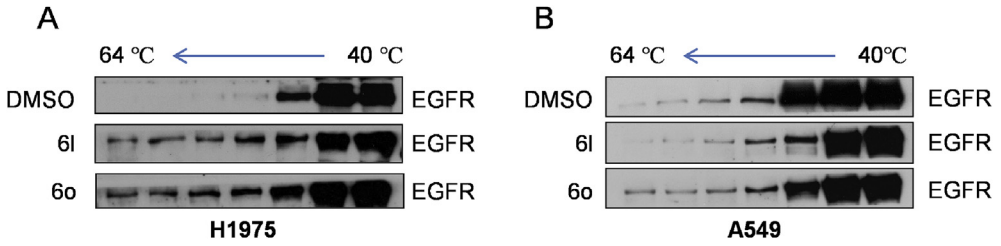

Fig. 6. Compounds **6l** and **6o** specifically bound to mutant EGFR protein at cellular level. H1975 (A) and A549 (B) cells were treated with **6o** and **6l** at 50 μM for 4 h followed by heating from 40 to 64 °C, using DMSO as the control. Western blot was used to detect the expression of EGFR protein. Three individual experiments were performed for each group.

Table 2
IC_{50} values of selected compounds against the tested cell lines.

Comp.		IC50(μM)			
		H1975	A549	PC9	L02
6a		4.15 ± 0.38	3.46 ± 0.39	5.78 ± 0.59	> 50
6d	>20	ND[a]	ND	ND	
6e	12.47 ± 0.86	ND	ND	ND	
6g	8.37 ± 4.58	14.51 ± 1.61	>20	> 50	
6j	6.76 ± 2.56	6.95 ± 2.70	>20	22.13 ± 2.34	
6k	4.40 ± 0.25	10.05 ± 0.80	>20	24.81 ± 4.18	
6l	5.60 ± 0.15	10.89 ± 0.22	10.37 ± 0.27	16.73 ± 2.50	
6m	7.99 ± 1.30	10.76 ± 2.50	8.08 ± 0.21	19.33 ± 2.31	
6n	5.23 ± 0.22	10.05 ± 2.91	5.34 ± 2.93	17.46 ± 3.63	
6o	3.20 ± 0.58	10.78 ± 0.72	2.92 ± 0.34	16.02 ± 1.23	
6p	>20	ND	>20	ND	
Gefitinib	7.14 ± 0.38	17.79 ± 4.94	0.007 ± 0.002	31.32 ± 4.24	
Erlotinib	7.25 ± 1.47	>20	0.008 ± 0.001	> 50	
Olmutinib	0.026 ± 0.01	9.61 ± 0.25	0.028 ± 0.022	16.51 ± 2.30	

[a] ND means no determined.

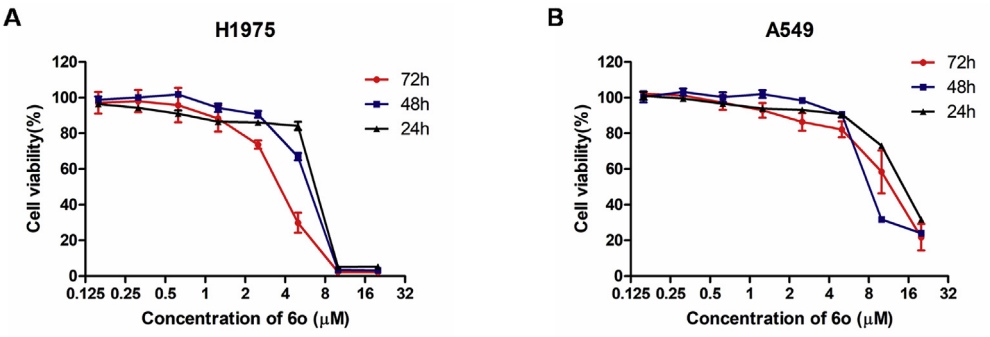

Fig. 7. Effect of compound **6o** on the cell viability of H1975 (A) and A549 (B) cells. Three individual experiments were performed for each group. The data were expressed as Mean ± SD.

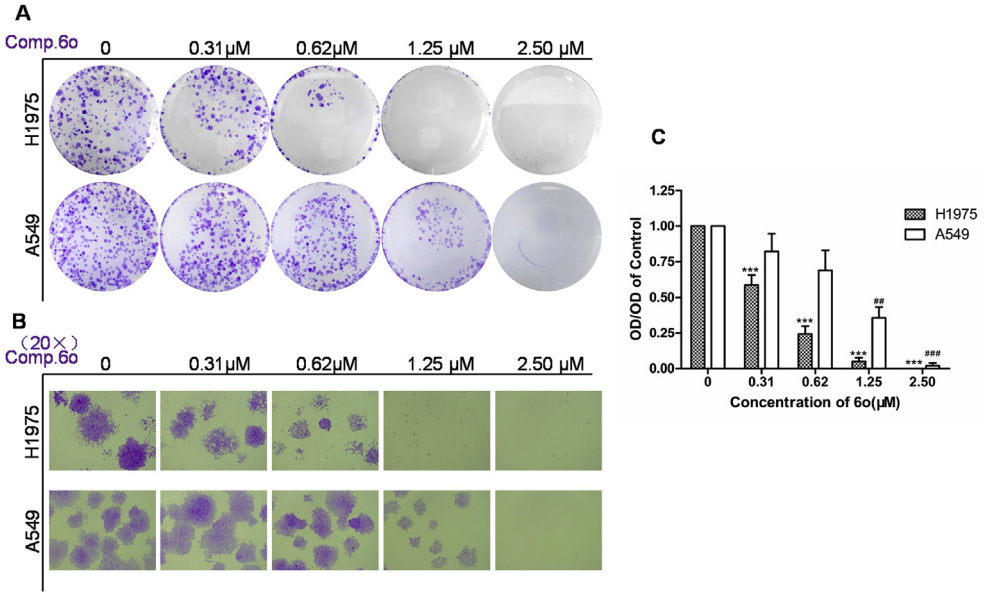

Fig. 8. Compound **6o** inhibited colony formation of H1975 and A549 cells. (A) H1975 and A549 cells were treated with compound **6o** at 0.31, 0.62, 1.25 and 2.50 μM, respectively for 10 days. The clonogenicity was monitored by stereomicroscope (20 ×) to see the size of single clone (B) and was quantified by measuring absorbance of crystal violet (C). Three individual experiments were performed for each group. The data were expressed as Mean ± SD. *$p < 0.05$, **$p < 0.01$, ***$p < 0.001$ compared with the control of H1975; $^{\#}p < 0.05$, $^{\#\#}p < 0.01$ compared with the control of A549. (For interpretation of the references to colour in this figure legend, the reader is referred to the Web version of this article.)

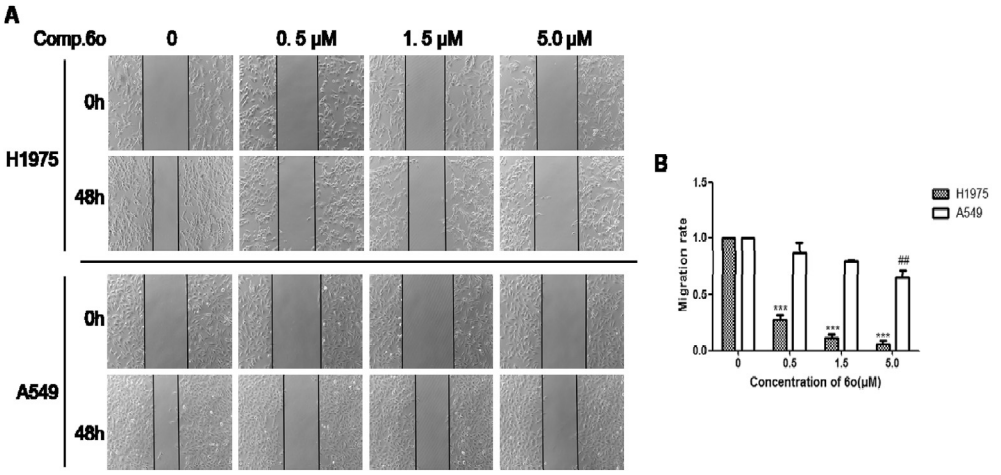

Fig. 9. Compound **6o** selectively inhibited the migration of H1975 cells. (A) H1975 and A549 cells were treated with compound **6o** at 0, 0.5, 1.5 and 5 μM for 48 h respectively. Their initial wounds before dosing were used as controls. (B) The migration rate was measured and quantitated with Image J. The area of the wound was precisely circled along the edge of the cell scratch for quantitative analysis. The migration rate = (0 h wound area − 48 h wound area)/0 h wound area. Three individual experiments were performed for each group. The data were expressed as the Mean ± SD. $^{*}p < 0.05$, $^{**}p < 0.01$, $^{***}p < 0.001$ compared with the control of H1975; $^{\#\#}p < 0.01$ compared with the control of A549.

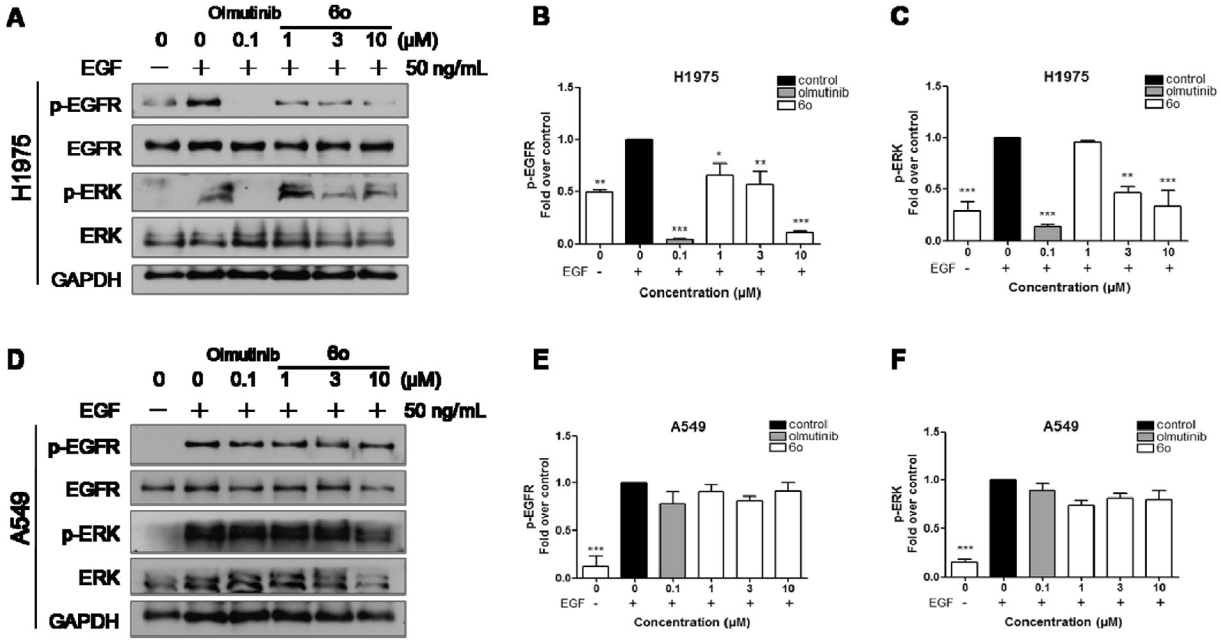

Fig. 10. Compound **6o** blocked EGFR signaling pathways in H1975 cells. H1975 and A549 cells were treated with **6o** at 0, 1, 3 and 10 μM for 2 h followed by exposure EGF for 10 min, with the olmutinib at 0.1 μM as a positive control and EGF + at 0 μM as control. Then Western blot analysis was subjected (A and D). Their quantitation was performed (B, C) and (E, F). Three individual experiments were performed for each group. The data was expressed as the Mean ± SD. $^{*}p < 0.05$, $^{**}p < 0.01$, $^{***}p < 0.001$, compared with the control.

pyrimidine compounds, especially **6l** and **6o**, may serve as the lead compounds for generating new series of the third-generation EGFR-TKIs, selectively targeting the mutant $EGFR^{L858R/T790M}$.

4. Experimental section

4.1. General

Solvents and reagents were purchased from commercial sources and were used without further purification. Thin layer chromatography (TLC) was made out with silica gel on glass plates and visualized under the UV light (254 nm). The products were purified by column chromatography over silica gel (200−300 mesh). Melting points were determined on an X-5 micromelting apparatus and are uncorrected. All the NMR spectra were recorded with a Bruker DPX 400 MHz spectrometer with TMS as an internal standard in $CDCl_3$ or DMSO-d_6. Chemical shifts are given as δ ppm values relative to TMS. HRMS were recorded on a Waters micromass Q-T of micromass spectrometer.

4.2. Experimental procedures

4.2.1. Synthesis of (E)-N-(3-methoxyphenyl)cinnamamide **(3)**

To a mixed solution of acetone (8 mL) and water (16 mL), 3-methoxyaniline (1 g, 8.12 mmol), potassium carbonate (1.68 g, 12.18 mmol), cinnamoyl chloride (1.62 g, 9.74 mmol) were added

sequentially. The reaction mixture was stirred in the ice bath for 30 min. Upon completion of the reaction, the mixture was poured into ice water and extracted with EtOAc for 3 times. The combined organic layers were dried over anhydrous $MgSO_4$, removal of the solvent gave compound **3**. White solid, yield: 98%, Mp 114–115 °C. ^{1}H NMR (400 MHz, DMSO-d_6) δ 10.19 (s, 1H), 7.61 (dd, J = 13.0, 12.1 Hz, 3H), 7.49–7.38 (m, 4H), 7.22 (dd, J = 8.8, 3.9 Hz, 2H), 6.83 (d, J = 15.7 Hz, 1H), 6.69–6.62 (m, 1H), 3.75 (s, 3H). ^{13}C NMR (100 MHz, DMSO-d_6) δ 163.53, 159.52, 140.39, 140.20, 134.68, 129.76, 129.55, 128.99, 127.69, 122.23, 111.55, 108.76, 105.08, 54.95.

*4.2.2. Synthesis of 7-hydroxyquinolin-2(1H)-one **(4)***

Aluminum trichloride (3.16 g, 23.69 mmol) was added in batches to a suspension of compound **3** (1 g, 3.95 mmol) in chlorobenzene (30 mL) cooled in ice bath. The reaction system was gradually warmed to 120 °C and refluxed for 3–5 h. After the reaction completed, the mixture was cooled to room temperature and concentrated, and the residue was purified by silica gel column chromatography to afford the desired compound **4**. Brown solid, yield: 54%, Mp > 300 °C. ^{1}H NMR (400 MHz, DMSO-d_6) δ 11.50 (s, 1H), 10.11 (s, 1H), 7.73 (d, J = 9.4 Hz, 1H), 7.44 (d, J = 8.5 Hz, 1H), 6.72–6.56 (m, 2H), 6.21 (d, J = 9.4 Hz, 1H). ^{13}C NMR (100 MHz, DMSO-d_6) δ 162.29, 160.06, 141.05, 140.45, 129.42, 116.07, 112.94, 112.46, 100.09. HRMS (ESI): m/z calcd for $C_9H_7NO_2$, $[M+H]^+$: 162.0555; found: 162.0552.

*4.2.3. Synthesis of 7-(2-chlorothieno[3,2-d]pyrimidin-4-yloxy) quinolin-2(1H)-one **(5)***

Compound **4** (0.7 g, 4.34 mmol) and 2,4-dichlorothieno[3,2-*d*] pyrimidine (1.07 g, 5.21 mmol) were added to a reaction flask, followed by addition of potassium carbonate (1.8 g, 13.03 mmol), water (10 mL), acetonitrile (50 mL), the mixture was kept under reflux for 2–5 h. The formed white solid was filtered and washed with dichloromethane and water for several times, and then dried under vacuum overnight to obtain compound **5**. White solid, yield: 78%, Mp > 300 °C. ^{1}H NMR (400 MHz, DMSO-d_6) δ 8.57 (d, J = 5.4 Hz, 1H), 7.90 (d, J = 9.5 Hz, 1H), 7.75 (d, J = 8.6 Hz, 1H), 7.65 (d, J = 5.4 Hz, 1H), 7.24 (d, J = 2.2 Hz, 1H), 7.14 (dd, J = 8.5, 2.3 Hz, 1H), 6.50 (d, J = 9.5 Hz, 1H). ^{13}C NMR (100 MHz, DMSO-d_6) δ 164.43, 163.92, 163.05, 154.81, 152.33, 141.50, 139.72, 139.15, 129.33, 123.51, 121.73, 117.73, 116.29, 115.28, 108.54. HRMS (ESI): m/z calcd for $C_{15}H_8ClN_3O_2S$, $[M+H]^+$: 330.0104; found: 330.0106.

*4.2.4. General procedure for the synthesis of compounds **6a-r***

Compound **5** (1.0 eq.) and amine derivative (1.0 eq.) were dissolved in dioxane (5 mL) and then $Pd_2(dba)_3$ (0.2 eq.), BINAP (0.2eq), Cesium carbonate (1.0eq.) were added. The reaction mixture was stirred at 100 °C until the reaction was done. The resultant mixture was concentrated, and the residue was purified by silica gel column chromatography to give the corresponding products **6a-r**.

*4.2.4.1. 7-(2-(4-(4-methylpiperazin-1-yl)phenylamino)thieno[3,2-d] pyrimidin-4-yloxy)quinolin-2(1H)-one **(6a)**.* Yellow solid, yield: 55%, Mp > 300 °C. ^{1}H NMR (400 MHz, DMSO-d_6) δ 11.88 (s, 1H), 9.23 (s, 1H), 8.27 (d, J = 5.4 Hz, 1H), 7.99 (d, J = 9.6 Hz, 1H), 7.80 (d, J = 8.5 Hz, 1H), 7.32 (d, J = 5.3 Hz, 3H), 7.25–7.13 (m, 2H), 6.62 (s, 2H), 6.53 (d, J = 9.6 Hz, 1H), 2.95 (s, 4H), 2.43 (d, J = 4.3 Hz, 4H), 2.21 (s, 3H). ^{13}C NMR (100 MHz, DMSO-d_6) δ 165.02, 163.47, 161.93, 157.82, 153.44, 145.87, 139.95, 139.88, 136.84, 132.46, 129.51, 123.16, 121.31, 120.08, 117.17, 116.45, 115.45, 108.37, 106.78, 54.55, 48.71, 45.66. HRMS (ESI): m/z calcd for $C_{26}H_{24}N_6O_2S$, $[M+H]^+$: 485.1760; found: 485.1762.

*4.2.4.2. 7-(2-(3-fluoro-4-morpholinophenylamino)thieno[3,2-d]pyrimidin-4-yloxy)quinolin-2(1H)-one **(6b)**.* Brown solid, yield: 51%, Mp > 300 °C. ^{1}H NMR (400 MHz, DMSO-d_6) δ 11.86 (s, 1H), 9.53 (s, 1H), 8.32 (d, J = 5.4 Hz, 1H), 7.99 (d, J = 9.6 Hz, 1H), 7.80 (d, J = 8.3 Hz, 1H), 7.54–7.42 (m, 1H), 7.39 (d, J = 5.4 Hz, 1H), 7.29–7.10 (m,3H), 6.75 (t, J = 8.9 Hz, 1H), 6.53 (d, J = 9.6 Hz, 1H), 3.76–3.62 (m, 4H), 2.90–2.78 (m, 4H). ^{13}C NMR (100 MHz, DMSO-d_6) δ 164.76, 163.53, 161.95, 157.31, 155.70, 153.31, 139.99, 139.90, 137.25, 135.92, 135.81, 133.45, 133.36, 129.60, 123.24, 121.38, 118.66, 117.30, 116.36, 114.57, 108.14, 106.91, 106.64, 66.16, 50.86. HRMS (ESI): m/z calcd for $C_{25}H_{20}FN_5O_3S$, $[M+H]^+$: 490.1349; found: 490.1347.

*4.2.4.3. 7-(2-(4-methylpiperazin-1-yl)thieno[3,2-d]pyrimidin-4-yloxy)quinolin-2(1H)-One **(6c)**.* Yellow solid, yield: 53%, Mp 237–238 °C. ^{1}H NMR (400 MHz, $CDCl_3$) δ12.24 (s, 1H), 7.83 (d, J = 9.7 Hz, 1H), 7.81 (d, J = 5.4 Hz, 1H), 7.60 (d, J = 8.6 Hz, 1H), 7.39 (d, J = 2.0 Hz, 1H), 7.23 (d, J = 5.4 Hz, 1H), 7.14 (dd, J = 8.6, 2.1 Hz, 1H), 6.69 (d, J = 9.5 Hz, 1H), 3.81 (s, 4H), 2.61 (s, 4H), 2.42 (s, 3H). ^{13}C NMR (100 MHz, $CDCl_3$) δ 165.48, 164.57, 163.43, 160.03, 154.14, 140.75, 139.42, 135.19, 128.70, 123.44, 120.72, 117.51, 108.79, 107.31, 54.42, 45.43, 43.47. HRMS (ESI): m/z calcd for $C_{20}H_{19}N_5O_2S$, $[M+H]^+$: 394.1338; found: 394.1340.

*4.2.4.4. 7-(2-(4-ethylpiperazin-1-yl)thieno[3,2-d]pyrimidin-4-yloxy) quinolin-2(1H)-one **(6d)**.* Yellow solid, yield: 46%, Mp 244–245 °C. ^{1}H NMR (400 MHz, $CDCl_3$) δ 12.64 (s, 1H), 7.82 (d, J = 9.5 Hz, 1H), 7.78 (d, J = 5.4 Hz, 1H), 7.59 (d, J = 8.6 Hz, 1H), 7.42 (d, J = 1.7 Hz, 1H), 7.22 (d, J = 5.4 Hz, 1H), 7.15 (dd, J = 8.6, 2.1 Hz, 1H), 6.68 (d, J = 9.5 Hz, 1H), 3.78–3.62 (m, 4H), 2.49–2.31 (m, 6H), 1.06 (t, J = 7.2 Hz, 3H). ^{13}C NMR (100 MHz, $CDCl_3$) δ 165.52, 164.76, 163.32, 160.31, 154.22, 140.70, 139.50, 134.89, 128.54, 123.43, 120.64, 117.58, 117.43, 108.91, 106.80, 52.64, 52.41, 44.21, 11.87. HRMS (ESI): m/z calcd for $C_{21}H_{21}N_5O_2S$, $[M+H]^+$: 408.1494; found: 408.1497.

*4.2.4.5. 7-(2-(4-morpholinophenylamino)thieno[3,2-d]pyrimidin-4-yloxy)quinolin-2(1H)-one **(6e)**.* Brown solid, yield: 41%, Mp 288–289 °C. ^{1}H NMR (400 MHz, DMSO-d_6) δ 11.85 (s, 1H), 9.23 (s, 1H), 8.28 (d, J = 4.2 Hz, 1H), 7.99 (d, J = 9.2 Hz, 1H), 7.80 (d, J = 8.1 Hz, 1H), 7.48–7.28 (m, 3H), 7.25–7.10 (m, 2H), 6.65 (s, 2H), 6.53 (d, J = 9.2 Hz, 1H), 3.70 (s, 4H), 2.93 (s, 4H). ^{13}C NMR (100 MHz, DMSO-d_6) δ 165.01, 163.46, 161.91, 157.82, 153.44, 145.91, 139.97, 139.86, 136.86, 132.80, 129.50, 123.18, 121.34, 120.09, 117.16, 116.42, 115.23, 108.31, 66.08, 49.18. HRMS (ESI): m/z calcd for $C_{25}H_{21}N_5O_3S$, $[M+H]^+$: 472.1443; found: 472.1445.

*4.2.4.6. 7-(2-(4-(1,4′-bipiperidin-1′-yl)phenylamino)thieno[3,2-d] pyrimidin-4-yloxy)quinolin-2(1H)-one **(6f)**.* Yellow solid, yeild: 47%, Mp 264–266 °C. ^{1}H NMR (400 MHz, DMSO-d_6) δ 11.86 (s, 1H), 9.19 (s, 1H), 8.27 (d, J = 5.4 Hz, 1H), 7.99 (d, J = 9.6 Hz, 1H), 7.80 (d, J = 8.5 Hz, 1H), 7.32 (d, J = 5.4 Hz, 3H), 7.25–7.12 (m, 2H), 6.67–6.51 (m, 3H), 2.34 (t, J = 10.4 Hz, 1H), 1.76 (d, J = 11.6 Hz, 2H), 1.58–1.43 (m, 8H), 1.43–1.24 (m, 5H), 1.22 (s, 3H).^{13}C NMR (100 MHz, DMSO) δ 165.05, 163.48, 161.96, 157.84, 153.46, 145.90, 139.93, 139.88, 136.85, 132.20, 129.51, 128.62, 123.14, 121.29, 120.14, 117.17, 116.46, 115.90, 108.39, 62.54, 61.75, 49.61, 49.11, 31.24, 28.96, 27.10, 25.68, 24.24, 22.04. HRMS (ESI): m/z calcd for $C_{31}H_{32}N_6O_2S$, $[M+H]^+$: 553.2386; found: 553.2383.

*4.2.4.7. 7-(2-(3-fluoro-4-(4-methylpiperazin-1-yl)phenylamino) thieno[3,2-d]pyrimidin-4-yloxy)quinolin-2(1H)-one **(6g)**.* Brown solid, yeild: 52%, Mp > 300 °C. ^{1}H NMR (400 MHz, DMSO-d_6) δ 11.83 (s, 1H), 9.49 (s, 1H), 8.32 (d, J = 5.4 Hz, 1H), 7.98 (d, J = 9.6 Hz, 1H), 7.80 (d, J = 8.4 Hz, 1H), 7.44 (s, 1H), 7.38 (d, J = 5.4 Hz, 1H), 7.24–7.13 (m, 3H), 6.73 (t, J = 9.0 Hz, 1H), 6.52 (d, J = 9.6 Hz, 1H), 2.85 (s, 4H), 2.45 (s, 4H), 2.22 (s, 3H). ^{13}C NMR (100 MHz, DMSO-d_6) δ 164.79,

163.54, 161.94, 157.34, 153.33, 139.99, 139.88, 137.22, 135.69, 129.59, 123.22, 121.37, 118.79, 117.30, 116.35, 114.54, 108.16, 106.67, 54.61, 50.20, 45.60. HRMS (ESI): *m/z* calcd for $C_{26}H_{23}FN_6O_2S$, $[M+H]^+$: 503.1665; found: 503.1663.

4.2.4.8. 7-((2-((4-(1,1-dioxidothiomorpholino)phenyl)amino)thieno[3,2-d]pyrimidin-4-yl)oxy)quinolin-2(1H)-one ***(6h)***. Pink solid, yield: 43%, Mp > 300 °C. ^{1}H NMR (400 MHz, DMSO-d_6) δ 11.87 (s, 1H), 9.27 (s, 1H), 8.28 (d, J = 5.4 Hz, 1H), 7.99 (d, J = 9.6 Hz, 1H), 7.81 (d, J = 8.5 Hz, 1H), 7.41 (s, 2H), 7.33 (d, J = 5.4 Hz, 1H), 7.23–7.15 (m, 2H), 6.72 (d, J = 7.5 Hz, 2H), 6.55 (d, J = 9.6 Hz, 1H), 3.61 (s, 4H), 3.13–3.03 (m, 4H). ^{13}C NMR (100 MHz, DMSO-d_6) δ 164.97, 163.48, 161.96, 157.74, 153.43, 142.40, 139.93, 136.94, 133.12, 129.53, 123.17, 121.36, 120.31, 117.18, 116.50, 116.15, 108.33, 49.75, 47.49. HRMS (ESI): *m/z* calcd for $C_{25}H_{21}N_5O_4S_2$, $[M+H]^+$: 520.1113; found: 520.1112.

4.2.4.9. 7-(2-(4-(morpholinomethyl)phenylamino)thieno[3,2-d]pyrimidin-4-yloxy)quinolin-2(1H)-one ***(6i)***. White solid, yield: 52%, Mp 269–271 °C. ^{1}H NMR (400 MHz, DMSO-d_6) δ 11.86 (s, 1H), 9.47 (s, 1H), 8.31 (d, J = 5.4 Hz, 1H), 8.00 (d, J = 9.6 Hz, 1H), 7.81 (d, J = 8.4 Hz, 1H), 7.47 (d, J = 7.5 Hz, 2H), 7.38 (d, J = 5.4 Hz, 1H), 7.20 (dt, J = 8.3, 2.2 Hz, 2H), 6.95 (d, J = 8.1 Hz, 2H), 6.54 (d, J = 9.6 Hz, 1H), 3.58–3.50 (m, 4H), 3.29 (s, 2H), 2.26 (s, 4H). ^{13}C NMR (100 MHz, DMSO-d_6) δ 164.87, 163.52, 161.90, 157.55, 153.41, 139.98, 139.84, 139.23, 137.12, 130.19, 129.50, 128.84, 123.22, 121.41, 118.49, 117.19, 116.45, 108.24, 107.44, 66.13, 61.98, 52.96. HRMS (ESI): *m/z* calcd for $C_{26}H_{23}N_5O_3S$, $[M+H]^+$: 486.1600; found: 486.1601.

4.2.4.10. 7-(2-(2-methoxy-4-(4-methylpiperazin-1-yl)phenylamino)thieno[3,2-d]pyrimidin-4-yloxy)quinolin-2(1H)-one ***(6j)***. White solid, yield: 44%, Mp 265–266 °C. ^{1}H NMR (400 MHz, DMSO-d_6) δ 11.87 (s, 1H), 8.27 (d, J = 5.4 Hz, 1H), 7.99 (d, J = 9.6 Hz, 1H), 7.85–7.70 (m, 2H), 7.57–7.36 (m, 1H), 7.31 (d, J = 5.4 Hz, 1H), 7.21 (d, J = 2.2 Hz, 1H), 7.17 (dd, J = 8.5, 2.3 Hz, 1H), 6.54 (dd, J = 5.9, 3.5 Hz, 2H), 6.15 (s, 1H), 3.75 (s, 3H), 3.10–2.91 (m, 4H), 2.48–2.36 (m, 4H), 2.23 (s, 3H). ^{13}C NMR (100 MHz, DMSO-d_6) δ 165.07, 163.42, 161.97, 158.19, 153.28, 150.66, 147.74, 139.85, 136.94, 129.43, 123.15, 121.28, 120.37, 117.12, 116.40, 108.19, 106.34, 99.94, 55.50, 54.53, 48.57, 45.62. HRMS (ESI): *m/z* calcd for $C_{27}H_{26}N_6O_3S$, $[M+H]^+$: 515.1865; found: 515.1866.

4.2.4.11. 7-(2-(4-(4-ethylpiperazin-1-yl)-2-methoxyphenylamino)thieno[3,2-d]pyrimidin-4-yloxy)quinolin-2(1H)-one ***(6k)***. Yellow solid, yield: 51%, Mp 271–273 °C. ^{1}H NMR (400 MHz, DMSO-d_6) δ 11.85 (s, 1H), 8.26 (d, J = 5.4 Hz, 1H), 7.97 (d, J = 9.6 Hz, 1H), 7.81–7.74 (m, 2H), 7.54–7.41 (m, 1H), 7.30 (d, J = 5.4 Hz, 1H), 7.21 (d, J = 2.2 Hz, 1H), 7.16 (dd, J = 8.5, 2.3 Hz, 1H), 6.53 (dd, J = 6.0, 3.5 Hz, 2H), 6.14 (d, J = 6.9 Hz, 1H), 3.74 (s, 3H), 3.06–2.96 (m, 4H), 2.48–2.41 (m, 4H), 2.35 (q, J = 7.2 Hz, 2H), 1.02 (t, J = 7.2 Hz, 3H). ^{13}C NMR (100 MHz, DMSO-d_6) δ 165.08, 163.42, 161.95, 158.18, 153.29, 150.61, 147.80, 139.89, 136.89, 129.40, 123.16, 122.31, 121.31, 120.37, 117.11, 116.36, 108.17, 106.98, 106.32, 99.90, 55.51, 52.31, 51.58, 48.76, 11.92. HRMS (ESI): *m/z* calcd for $C_{28}H_{28}N_6O_3S$, $[M+H]^+$: 529.2022; found: 529.2021.

4.2.4.12. 7-(2-(4-(1,4′-bipiperidin-1′-yl)-3-fluorophenylamino)thieno[3,2-d]pyrimidin-4-yloxy)quinolin-2(1H)-one ***(6l)***. Yellow solid, yield: 40%, Mp 245–246 °C. ^{1}H NMR (400 MHz, DMSO-d_6) δ 11.85 (s, 1H), 9.50 (s, 1H), 8.32 (d, J = 5.4 Hz, 1H), 7.98 (d, J = 9.6 Hz, 1H), 7.80 (d, J = 8.5 Hz, 1H), 7.50–7.35 (m, 2H), 7.23 (d, J = 2.2 Hz, 1H), 7.18 (dd, J = 8.5, 2.3 Hz, 2H), 6.74 (t, J = 9.1 Hz, 1H), 6.53 (d, J = 9.6 Hz, 1H), 3.23 (d, J = 11.7 Hz, 3H), 2.80 (s, 4H), 2.55 (d, J = 11.5 Hz, 2H), 1.92 (d, J = 11.5 Hz, 2H), 1.72–1.57 (m, 6H), 1.46 (d, J = 4.7 Hz, 2H). ^{13}C NMR (100 MHz, DMSO-d_6) δ = 164.78, 163.54, 161.95, 157.33, 155.67, 153.32, 153.26, 140.00, 139.89, 137.25, 135.80, 135.69, 133.54, 133.45, 129.58, 123.21, 121.36, 119.11, 117.30, 116.34, 114.53, 108.16, 107.55, 106.87, 106.61, 61.91, 50.13, 49.32, 26.86, 24.33, 23.06, 21.04. HRMS (ESI): *m/z* calcd for $C_{31}H_{31}FN_6O_2S$, $[M+H]^+$: 571.2291; found: 571.2290.

4.2.4.13. 7-(2-(4-((4-methylpiperazin-1-yl)methyl)phenylamino)thieno[3,2-d]pyrimidin-4-yloxy)quinolin-2(1H)-one ***(6m)***. Yellow solid, yield: 59%, Mp 235–237 °C. ^{1}H NMR (400 MHz, DMSO-d_6) δ 11.85 (s, 1H), 9.45 (s, 1H), 8.31 (d, J = 5.4 Hz, 1H), 7.99 (d, J = 9.6 Hz, 1H), 7.80 (d, J = 8.5 Hz, 1H), 7.47 (d, J = 7.8 Hz, 2H), 7.37 (d, J = 5.4 Hz, 1H), 7.22 (d, J = 2.1 Hz, 1H), 7.19 (dd, J = 8.4, 2.3 Hz, 1H), 6.94 (d, J = 8.1 Hz, 2H), 6.53 (d, J = 9.6 Hz, 1H), 3.29 (s, 2H), 2.28 (s, 8H), 2.14 (s, 3H). ^{13}C NMR (100 MHz, DMSO-d_6) δ 164.87, 163.50, 161.87, 157.58, 153.42, 140.00, 139.80, 139.15, 137.09, 130.73, 129.47, 128.73, 123.22, 121.44, 118.50, 117.17, 116.43, 108.19, 107.45, 61.58, 54.61, 52.24, 45.61. HRMS (ESI): *m/z* calcd for $C_{27}H_{26}N_6O_2S$, $[M+H]^+$: 499.1916; found: 499.1917.

4.2.4.14. 7-(2-(4-((4-ethylpiperazin-1-yl)methyl)phenylamino)thieno[3,2-d]pyrimidin-4-yloxy)quinolin-2(1H)-one ***(6n)***. Yellow solid, yield: 59%, Mp 247–248 °C. ^{1}H NMR (400 MHz, DMSO-d_6) δ 11.87 (s, 1H), 9.45 (s, 1H), 8.30 (d, J = 5.4 Hz, 1H), 7.99 (d, J = 9.6 Hz, 1H), 7.81 (d, J = 8.5 Hz, 1H), 7.46 (d, J = 7.6 Hz, 2H), 7.37 (d, J = 5.4 Hz, 1H), 7.23 (d, J = 2.2 Hz, 1H), 7.19 (dd, J = 8.5, 2.3 Hz, 1H), 6.94 (d, J = 8.1 Hz, 2H), 6.53 (d, J = 9.6 Hz, 1H), 3.31 (s, 2H), 2.47–2.08 (m, 10H), 1.00 (t, J = 7.2 Hz, 3H). ^{13}C NMR (100 MHz, DMSO-d_6) δ 164.87, 163.52, 161.94, 157.55, 153.42, 139.95, 139.88, 139.20, 137.12, 130.36, 129.50, 128.81, 123.21, 121.38, 118.50, 117.20, 116.48, 108.24, 107.44, 61.37, 51.92, 51.76, 51.38, 11.41. HRMS (ESI): *m/z* calcd for $C_{28}H_{28}N_6O_2S$, $[M+H]^+$: 513.2073; found: 513.2075.

4.2.4.15. 7-(2-(4-(2-(dimethylamino)ethylamino)-3-fluorophenylamino)thieno[3,2-d]pyrimidin-4-yloxy)quinolin-2(1H)-one ***(6o)***. Yellow solid, yield: 49%, Mp 257–259 °C. ^{1}H NMR (400 MHz, DMSO-d_6) δ 11.85 (s, 1H), 9.28 (s, 1H), 8.29 (d, J = 5.4 Hz, 1H), 7.97 (d, J = 9.6 Hz, 1H), 7.79 (d, J = 8.5 Hz, 1H), 7.36 (t, J = 10.4 Hz, 2H), 7.22 (d, J = 2.1 Hz, 1H), 7.18 (dd, J = 8.5, 2.3 Hz, 1H), 7.10 (s, 1H), 6.49 (dd, J = 20.5, 9.6 Hz, 2H), 4.62 (s, 1H), 3.02 (dd, J = 11.8, 5.9 Hz, 2H), 2.41 (t, J = 6.4 Hz, 2H), 2.15 (s, 6H). ^{13}C NMR (100 MHz, DMSO-d_6) δ 164.93, 163.46, 161.90, 157.64, 153.37, 151.35, 149.01, 140.02, 139.84, 136.97, 131.33, 131.21, 130.12, 130.02, 129.52, 123.17, 121.39, 117.19, 116.33, 115.32, 111.86, 108.04, 106.53, 106.28, 57.62, 45.07, 40.76. HRMS (ESI): *m/z* calcd for $C_{25}H_{23}FN_6O_2S$, $[M+H]^+$: 491.1665; found: 491.1663.

4.2.4.16. 7-(2-(5-(4-methylpiperazin-1-yl)pyridin-2-ylamino)thieno[3,2-d]pyrimidin-4-yloxy)quinolin-2(1H)-one ***(6p)***. White solid, yield: 40%, Mp > 300 °C. ^{1}H NMR (400 MHz, DMSO-d_6) δ 11.84 (s, 1H), 9.36 (s, 1H), 8.32 (d, J = 5.4 Hz, 1H), 8.00 (d, J = 9.6 Hz, 1H), 7.89 (d, J = 2.9 Hz, 1H), 7.81 (d, J = 8.6 Hz, 1H), 7.59 (d, J = 9.1 Hz, 1H), 7.38 (d, J = 5.4 Hz, 1H), 7.26 (d, J = 2.2 Hz, 1H), 7.20 (dd, J = 8.5, 2.3 Hz, 1H), 6.91 (dd, J = 9.1, 2.8 Hz, 1H), 6.53 (d, J = 9.5 Hz, 1H), 3.06–2.93 (m, 4H), 2.47–2.38 (m, 4H), 2.21 (s, 3H). ^{13}C NMR (100 MHz, DMSO-d_6) δ 164.90, 163.43, 161.94, 156.85, 153.35, 145.35, 142.37, 139.89, 137.27, 135.23, 129.48, 124.29, 123.24, 121.32, 117.15, 116.40, 113.62, 108.30, 107.76, 54.31, 48.34, 45.65. HRMS (ESI): *m/z* calcd for $C_{25}H_{23}N_7O_2S$, $[M+H]^+$: 486.1712; found: 486.1712.

4.2.4.17. 7-(2-(4-fluorophenylamino)thieno[3,2-d]pyrimidin-4-yloxy)quinolin-2(1H)-one ***(6q)***. White solid, yield: 49%, Mp > 300 °C. ^{1}H NMR (400 MHz, DMSO-d_6) δ 11.87 (s, 1H), 9.49 (s, 1H), 8.31 (d, J = 5.4 Hz, 1H), 8.00 (d, J = 9.6 Hz, 1H), 7.81 (d, J = 8.4 Hz, 1H), 7.57 (dd, J = 7.6, 4.9 Hz, 2H), 7.38 (d, J = 5.4 Hz, 1H), 7.20 (dt, J = 8.4, 2.2 Hz, 2H), 6.88 (t, J = 8.7 Hz, 2H), 6.54 (d,

J = 9.6 Hz, 1H). ^{13}C NMR (100 MHz, DMSO-d_6) δ 164.77, 163.49, 161.96, 158.06, 157.47, 155.70, 153.37, 139.93, 137.18, 136.79, 136.77, 129.53, 123.23, 121.38, 120.27, 120.19, 117.19, 116.49, 114.67, 114.45, 108.11, 107.70. HRMS (ESI): m/z calcd for $C_{21}H_{13}FN_4O_2S$, $[M+H]^+$: 405.0821; found: 405.0822.

4.2.4.18. 7-(2-(3-methoxyphenylamino)thieno[3,2-d]pyrimidin-4-yloxy)quinolin-2(1H)-one ***(6r)***. White solid, yield: 46%, Mp 282–284 °C. ^{1}H NMR (400 MHz, DMSO-d_6) δ 11.83 (s, 1H), 9.47 (s, 1H), 8.33 (d, J = 5.4 Hz, 1H), 7.98 (d, J = 9.6 Hz, 1H), 7.79 (d, J = 8.5 Hz, 1H), 7.40 (d, J = 5.4 Hz, 1H), 7.30 (s, 1H), 7.22 (d, J = 2.1 Hz, 1H), 7.19 (dd, J = 8.5, 2.2 Hz, 1H), 7.15 (d, J = 8.0 Hz, 1H), 6.96 (t, J = 8.1 Hz, 1H), 6.53 (d, J = 9.6 Hz, 1H), 6.43 (dd, J = 8.1, 2.1 Hz, 1H), 3.57 (s, 3H). ^{13}C NMR (100 MHz, DMSO-d_6) δ 164.74, 163.42, 161.91, 159.40, 157.51, 153.37, 141.56, 140.04, 139.86, 137.21, 129.56, 128.83, 123.27, 121.38, 117.22, 116.26, 111.09, 107.94, 107.79, 106.16, 104.71, 54.69. HRMS (ESI): m/z calcd for $C_{22}H_{16}N_4O_3S$, $[M+H]^+$: 417.1021; found: 417.1022.

4.3. Biological evaluation

4.3.1. Materials

All compounds were dissolved in DMSO to make a 10 mM stock solution. RPMI-1640 was purchased from Biological Industries. MTT was also purchased from Solarbio. Fetal Bovine Serum (FBS) was obtained from Tianhang Biotechnology Co. ERK primary antibodies were purchased from SAB. EGFR, p-EGFR (P-Tyr1068), p-ERK (Thr202/Tyr204) primary antibodies were purchased from CST. EGF was purchased from Sino Biological.

4.3.2. Cell culture

Human cancer cells H1975, A549, PC9, and human normal cells L02 were obtained from Zhengzhou University and maintained in RPMI-1640 complete medium (which supplemented with 10% FBS and 100 U/mL penicillin and 100 g/mL streptomycin antibiotics) at 37 °C in a 5% CO_2 humidified atmosphere.

4.3.3. Kinase inhibition assay of EGFR $^{L858R/T790M}$ and EGFR^{WT}

Mobility shift assay was used in this study. Kinase binding to ATP causes the kinase reaction and the fluorescently labeled EGFR substrate Kinase substrate 22 is phosphorylated into the product resulting in a charge difference. If the compound inhibits the binding of ATP to the kinase, the phosphorylated product will be correspondingly reduced. Based on this charge difference, Caliper EZ Reader is used to separate and detect the conversion of product by capillary electrophoresis. EGFR and EGFR$^{L858R/T790M}$ kinase were purchased from Carna Biosciences. The kinase (2.5 nM) were assayed with test compounds in a final volume of 25 μL, 3 μL kinase peptide 22 (5-FAM-EEPLYWSFPAKKK-CONH2), 1.4 μM and 20 μL ATP for EGFR and EGFR-L858R/T790M respectively. Reaction buffer contains 50 mM HEPES, 0.01% Triton X-100, 10 mM $MgCl_2$ and 2 mM DL-dithiothreitol (DTT). After incubate at RT for 20 min, the reactions were stopped by adding 30 μL stop buffer (100 mM HEPES, 0.015% Brij-35, 50 mM EDTA). The reaction mixture was analyzed with Caliper EZ Reader and the conversion values were converted to inhibition. The log-inhibitor *vs*. response-Variable slope was calculated, usingthe GraphPad Prism 5.0 software to obtain the IC_{50} value of each compound for the enzyme activity.

4.3.4. Molecular docking studies

All the procedure was performed in MOE 2015.10. Cocrystal structures of 4-(4-{[2-{[(3S)-1-acetylpyrrolidin-3-yl]amino}-9-(propan-2-yl)-9*H*-purin-6-yl]amino}phenyl)-1-methylpiperazin-1-ium (a reversible EGFR$^{L858R/T790M}$ inhibitor) in EGFR$^{L858R/T790M}$ mutant (PDB ID: 5UGA) and WT EGFR (PDB ID: 5UGB) [25] were used as receptor structures and prepared by default parameters using QuickPrep module. The protonation states of the ionizable residues were adjusted at pH = 7. The three-dimensional structures of olmutinib, compounds **6l** and **6o** were generated by taking energy minimization and conformational search before docking. Binding site residues were defined by centering the box on the existing inhibitor in the complex. The covalent reaction type Michael addition was chosen and C797 in the receptor was defined as the covalently bound reactive residue. For each molecule, top 10 scored poses were generated by the program and were carefully visualized, among which the best scored pose was used to illustrate binding characteristics in the EGFR kinase.

4.3.5. Cellular thermal shift assay

Cells in the logarithmic growth phase were plated at a density of 70% into sterile cell culture dishes. After the cells were grown to a density of more than 80%, fresh medium containing the test compounds at 50 μM was added and an equal volume of DMSO was added to another dish as a negative control. After being placed in the incubator for 4 h, the cells were digested and collected. The cells were washed twice with PBS and 500 μL PBS was added to each tube. The cell suspension was divided into seven 200 μL EP tubes and placed in a PCR machine. The temperature gradient program was set as: 64.0, 62.5, 59.8, 55.0, 49.2, 44.6, 40.0 °C for 5 min. The cells were then transferred to 1.5 mL EP tubes and centrifuged for 4000 rpm for 5 min. These cells were subjected to normal protein extraction treatment and Western blot assay.

4.3.6. MTT assay

The MTT assay was carried out, following our previously reported methods [31]. Cells were seeded in 96-well plates (NEST Biotechnology, China) at a density of 2.0–4.0 × 10^3 cells per well and incubated overnight, followed by treatment with serial dilutions of the compounds (0.16–20 μM) 200 μL/well and incubated for 72 h. 20 μL MTT reagent (5 mg/ml, Solarbio) was added to each well, the cells were incubated for another 4 h. Then, the medium was removed and the formazan was dissolved in 150 μL DMSO. After shaking for 10 min, absorbance values were measured at 490 nm in an enzyme-linked immunosorbent assay reader (BioTek, USA). The cellular inhibition rate was calculated as follows: inhibition rate = 1- [($OD_{\text{treated group}} - OD_{\text{blank group}}$)/($OD_{\text{normal group}} - OD_{\text{blank group}}$)] × 100%. The drug concentrations required to inhibit cell growth by 50% (IC_{50}) was determined from concentration-response curves created with SPSS 17.0 software. The results are reported as the mean ± SD of three independent experiments. The cell viability curves at different concentrations of compound **6o** were created with GraphPad Prism 5.0 software.

4.3.7. Colony formation assay

Firstly, cells were seeded at 500 cells/well in six-well plates and put in carbon dioxide incubator overnight. Then, the cells were treated with 0, 0.31, 0.62, 1.25 and 2.50 μM **6o** for 10 days [32]. Every three days, the new medium was replaced including **6o**. After washing with PBS (phosphate-buffered saline), the cells were fixed with cold methanol and stained with crystal violet solution, then washed off the float with distilled water. Images were photographed after drying the plates overnight. The crystal violet crystals were dissolved by adding 75% ethanol. The absorbance at 595 nm was measured by an enzyme-linked immunosorbent assay reader. Data were analyzed using the GraphPad Prism 5.0 software.

4.3.8. Wound healing assay

H1975 and A549 cells were seeded into six-well plates with a density of 70–80%. After the cells were attached to the wall, drew a straight line along the ruler with a yellow pipette tip and washed

twice with PBS, added fresh 2% FBS medicated medium at 0, 0.5, 1.5 and 5.0 μM of **6o** [33]. The photos were taken under the microscope as the initial control and recorded the position of the photographs. After 2 days of culture, washed cells with PBS followed by take pictures at corresponding position. The area of the wound was precisely circled along the edge of the cell scratch for quantitative analysis. The migration rate = (0 h wound area − 48 h wound area)/ 0 h wound area.

4.3.9. Western blot analysis

Cells were seeded in six-well plates. After adhered to the bottom, texted cells were starved in a 1640 medium containing 1% penicillin/streptomycin for 24 h, then administration **6o** at 0, 1, 3 and 10 μM for 2 h followed by exposure EGF for 10 min [34]. Then the cells were collected and lysed by radio immunoprecipitation assay (RIPA) lysis buffer. Total proteins were extracted and separated by 8%–15% SDS-PAGE, and transferred on a nitrocellulose (NC) filter membrane. The membranes were blocked in 5% skim milk for 2 h at room temperature, and then incubated overnight at 4 °C with primary antibodies (1:1000–1:2000). After washing in PBST (4 × 8 min), membranes were incubated with horseradish-peroxidase-conjugated secondary antibody (1:5000) at room temperature for 2 h. Finally, the membranes were washed in PBST (4 × 8 min). The antibody-reactive bands were revealed by enhanced chemiluminescence (ECL) and exposed on Kodak radiographic film and the signal intensity of each band was determined using Image J software. All experiments were performed in triplicate.

4.4. Statistical analysis

Results were expressed as mean ± standard deviation (SD). Statistical analysis was performed using One-Way ANOVA for more than two group comparison. $P < 0.05$ was considered statistically significant.

Declaration of competing interest

I have no declaration of interest.

Acknowledgement

This work was supported by the National Key Grant from Chinese Ministry of Science and Technology (No. 2016YFA0501800 for Wen Zhao), the National Natural Science Foundation of China (Nos. 81470524 and 81870297 for Wen Zhao, Nos. 81703326 and 81973177 for Bin Yu), the Henan Scientific Innovation Talent Team, Department of Education (19IRTSTHN001 for Wen Zhao), the China Postdoctoral Science Foundation (Nos. 2018M630840 and 2019T120641 for Bin Yu).

Appendix A. Supplementary data

Supplementary data to this article can be found online at https://doi.org/10.1016/j.ejmech.2020.112388.

References

[1] R.L. Siegel, K.D. Miller, A. Jemal, Cancer statistics, 2020, Ca - Cancer J. Clin. 70 (2020) 7–30.
[2] R.L. Siegel, K.D. Miller, A. Jemal, Cancer statistics, 2018, A Cancer Journal for Clinicians 68 (2018) 7–30.
[3] J.P. van Meerbeeck, D.A. Fennell, D.K. De Ruysscher, Small-cell lung cancer, Lancet 378 (2011) 1741–1755.
[4] N.E. Hynes, H.A. Lane, ERBB receptors and cancer: the complexity of targeted inhibitors, Nat. Rev. Canc. 5 (2005) 341–354.
[5] M.H. Cohen, G.A. Williams, R. Sridhara, G. Chen, W.J. McGuinn, D. Morse, S. Abraham, A. Rahman, C. Liang, R. Lostritto, A. Baird, R. Pazdur, United States food and drug administration drug approval summary: gefitinib (ZD1839; iressa) tablets, Clin. Canc. Res. 10 (2004) 1212–1218.
[6] M.H. Cohen, J.R. Johnson, Y.F. Chen, R. Sridhara, R. Pazdur, FDA drug approval summary: erlotinib (Tarceva) tablets, Oncol. 10 (2005) 461–466.
[7] J.C. Yang, J. Shih, W. Su, T. Hsia, C. Tsai, S.I. Ou, C. Yu, G. Chang, C. Ho, L.V. Sequist, A.Z. Dudek, M. Shahidi, X.J. Cong, R.M. Lorence, P. Yang, V.A. Miller, Afatinib for patients with lung adenocarcinoma and epidermal growth factor receptor mutations (LUX-Lung 2): a phase 2 trial, Lancet Oncol. 13 (2012) 539–548.
[8] V.D. Cataldo, D.L. Gibbons, R. Perez-Soler, A. Quintas-Cardama, Treatment of non-small-cell lung cancer with erlotinib or gefitinib, N. Engl. J. Med. 364 (2011) 947–955.
[9] W. Pao, V.A. Miller, K.A. Politi, G.J. Riely, R. Somwar, M.F. Zakowski, M.G. Kris, H. Varmus, Acquired resistance of lung adenocarcinomas to gefitinib or erlotinib is associated with a second mutation in the EGFR kinase domain, PLoS Med. 2 (2005) e73.
[10] P.C. Lee, Y.F. Fang, H. Yamaguchi, W.J. Wang, T.C. Chen, X. Hong, B. Ke, W. Xia, Y. Wei, Z. Zha, Y. Wang, H.P. Kuo, C.W. Wang, C.Y. Tu, C.H. Chen, W.C. Huang, S.F. Chiang, L. Nie, J. Hou, C.T. Chen, L. Huo, W.H. Yang, R. Deng, K. Nakai, Y.H. Hsu, S.S. Chang, T.J. Chiu, J. Tang, R. Zhang, L. Wang, B. Fang, T. Chen, K.K. Wong, J.L. Hsu, M.C. Hung, Targeting PKCdelta as a therapeutic strategy against heterogeneous mechanisms of EGFR inhibitor resistance in EGFR-mutant lung cancer, Canc. Cell 34 (2018) 954–969.
[11] A.L.C. Agero, S.W. Dusza, C. Benvenuto-Andrade, K.J. Busam, P. Myskowski, A.C. Halpern, Dermatologic side effects associated with the epidermal growth factor receptor inhibitors, J. Am. Acad. Dermatol. 55 (2006) 657–670.
[12] C. Tan, D. Gilligan, S. Pacey, Treatment approaches for EGFR-inhibitor-resistant patients with non-small-cell lung cancer, Lancet Oncol. 16 (2015) E447–E459.
[13] T. Li, R. Perez-Soler, Skin toxicities associated with epidermal growth factor receptor inhibitors, Targeted Oncol. 4 (2009) 107–119.
[14] O. Juan, S. Popat, Treatment choice in epidermal growth factor receptor mutation-positive non-small cell lung carcinoma: latest evidence and clinical implications, Ther. Adv. Med. Oncol. 9 (2017) 201–216.
[15] P.A. Jaenne, J.C. Yang, D. Kim, D. Planchard, Y. Ohe, S.S. Ramalingam, M. Ahn, S. Kim, W. Su, L. Horn, D. Haggstrom, E. Felip, J. Kim, P. Frewer, M. Cantarini, K.H. Brown, P.A. Dickinson, S. Ghiorghiu, M. Ranson, AZD9291 in EGFR inhibitor-resistant non-small-cell lung cancer. *New england Journal of medicine* 372 (2015) 1689–1699. NSCLC: Current developments in medicinal chemistry. Medicinal Research Reviews, 38 (2018) 1550-1581.
[16] X. Lu, L. Yu, Z. Zhang, X. Ren, J.B. Smaill, K. Ding, Targeting EGFR (L858R/T790M) and EGFR (L858R/T790M/C797S) resistance mutations in epidermal growth factor receptor (EGFR) mutant selective inhibitor, in non-small cell lung cancer (NSCLC) patients having an activating EGFR mutation but failed to prior EGFR tyrosine kinase inhibitor (TKI) therapy, J. Thorac. Oncol. 82 (2013) S892–S893.
[17] S. Wang, S. Cang, D. Liu, Third-generation inhibitors targeting EGFR T790M mutation in advanced non-small cell lung cancer, J. Hematol. Oncol. 9 (2016) 34.
[18] E.S. Kim Olmutinib, First global approval (vol 76, pg 1153, 2016), Drugs 76 (2016) 1233.
[19] D. Kim, S. Kim, T.M. Kim, S. Lee, C. Choi, B. Keam, J.C. Lee, D. Heo, J. Lee, K. Yu, I. Jang, K.J. Lim, J. Son, D.H. Lee. Phase I Study of HM61713, a Novel
[20] J. Wang, X. Cheng, Y. Lu, B. Zhou, A case report of toxic epidermal necrolysis associated with AZD-9291, Drug Des. Dev. Ther. 12 (2018) 2163–2167.
[21] G. Xia, W. Chen, J. Zhang, J. Shao, Y. Zhang, W. Huang, L. Zhang, W. Qi, X. Sun, B. Li, Z. Xiang, C. Ma, J. Xu, H. Deng, Y. Li, P. Li, H. Miao, J. Han, Y. Liu, J. Shen, Y. Yu, A chemical tuned strategy to develop novel irreversible EGFR-TK inhibitors with improved safety and pharmacokinetic profiles, J. Med. Chem. 57 (2014) 9889–9900.
[22] Y. Jia, C.H. Yun, E. Park, D. Ercan, M. Manuia, J. Juarez, C. Xu, K. Rhee, T. Chen, H. Zhang, S. Palakurthi, J. Jang, G. Lelais, M. DiDonato, B. Bursulaya, P.Y. Michellys, R. Epple, T.H. Marsilje, M. McNeill, W. Lu, J. Harris, S. Bender, K.K. Wong, P.A. Janne, M.J. Eck, Overcoming EGFR(T790M) and EGFR(C797S) resistance with mutant-selective allosteric inhibitors, Nature 534 (2016) 129–132.
[23] C. Ricordel, L. Friboulet, F. Facchinetti, J.C. Soria, Molecular mechanisms of acquired resistance to third-generation EGFR-TKIs in EGFR T790M-mutant lung cancer, Ann. Oncol. : Off. J.Eur. Soc. Med. Oncol. 29 (2018) i28–i37.
[24] W. Zhao, B. Yu, Y. Chen, Quinolinone-containing Pyrimido Five-Membered Heyerocyclic Compound, Preparation Method and Application Thereof, 2019, pp. 12–13.
[25] S. Planken, D.C. Behenna, S.K. Nair, T.O. Johnson, A. Nagata, C. Almaden, S. Bailey, T.E. Ballard, L. Bernier, H. Cheng, S. Cho-Schultz, D. Dalvie, J.G. Deal, D.M. Dinh, M.P. Edwards, R.A. Ferre, K.S. Gajiwala, M. Hemkens, R.S. Kania, J.C. Kath, J. Matthews, B.W. Murray, S. Niessen, S.T. Orr, M. Pairish, N.W. Sach, H. Shen, M. Shi, J. Solowiej, K. Tran, E. Tseng, P. Vicini, Y. Wang, S.L. Weinrich, R. Zhou, M. Zientek, L. Liu, Y. Luo, S. Xin, C. Zhang, N-((3R,4R)-4-Fluoro-1-(6-((3-methoxy-1-methyl-1H-pyrazol-4-yl) amino)-9-methyl-9H-purin-2-yl) pyrrolidine-3-yl)acrylamide (PF-06747775) through structure-based drug design: a high affinity irreversible inhibitor targeting oncogenic EGFR mutants with selectivity over wild-type EGFR, J. Lafontaine. Discovery of, J. Med. Chem. 60 (2017) 3002–3019.
[26] S. Sogabe, Y. Kawakita, S. Igaki, H. Iwata, H. Miki, D.R. Cary, T. Takagi, S. Takagi,

Y. Ohta, T. Ishikawa, Structure-based approach for the discovery of pyrrolo [3,2-d]pyrimidine-based EGFR T790M/L858R mutant inhibitors, ACS Med. Chem. Lett. 4 (2013) 201–205.
[27] C.H. Yun, T.J. Boggon, Y. Li, M.S. Woo, H. Greulich, M. Meyerson, M.J. Eck, Structures of lung cancer-derived EGFR mutants and inhibitor complexes: mechanism of activation and insights into differential inhibitor sensitivity, Canc. Cell 11 (2007) 217–227.
[28] S. Yoshikawa, M. Kukimoto-Niino, L. Parker, N. Handa, T. Terada, T. Fujimoto, Y. Terazawa, M. Wakiyama, M. Sato, S. Sano, T. Kobayashi, T. Tanaka, L. Chen, Z.J. Liu, B.C. Wang, M. Shirouzu, S. Kawa, K. Semba, T. Yamamoto, S. Yokoyama, Structural basis for the altered drug sensitivities of non-small cell lung cancer-associated mutants of human epidermal growth factor receptor, Oncogene 32 (2013) 27–38.
[29] N.I. Kozlova, G.E. Morozevich, N.A. Ushakova, N.M. Gevorkian, A.E. Berman, Differences between integrin α5β1 and EGRF receptor in signal pathways controlling proliferation and apoptosis of MCF-7/Dox human breast carcinoma cells, Biochemistry (Moscow) Supplement Series B: Biomedical Chemistry 10 (2016) 276–282.
[30] R.A. Soo, S.M. Lim, N.L. Syn, R. Teng, R. Soong, T.S.K. Mok, B.C. Cho, Immune checkpoint inhibitors in epidermal growth factor receptor mutant non-small cell lung cancer: current controversies and future directions, Lung Canc. 115 (2018) 12–20.
[31] L. Li, J. Peng, W. Zhou, H. Qiao, X. Deng, Z. Li, J. Li, Y. Fu, S. Li, K. Sun, H. Liu, W. Zhao, Potent hydrazone derivatives targeting esophageal cancer cells, Eur. J. Med. Chem. 148 (2018) 359–371.
[32] Y. Lai, S. Lin, Y. Wu, H. Chen, J.J.W. Chen, AC-93253 iodide, a novel Src inhibitor, suppresses NSCLC progression by modulating multiple Src-related signaling pathways, J. Hematol. Oncol. 10 (2017) 172–185.
[33] B. Lin, X. Song, D. Yang, D. Bai, Y. Yao, N. Lu, Anlotinib inhibits angiogenesis &ITvia&IT suppressing the activation of VEGFR2, PDGFR beta and FGFR1, Gene 654 (2018) 77–86.
[34] Y. Zhang, L. Chen, H. Xu, X. Li, L. Zhao, W. Wang, B. Li, X. Zhang, 6,7-Dimorpholinoalkoxy quinazoline derivatives as potent EGFR inhibitors with enhanced antiproliferative activities against tumor cells, Eur. J. Med. Chem. 147 (2018) 77–89.